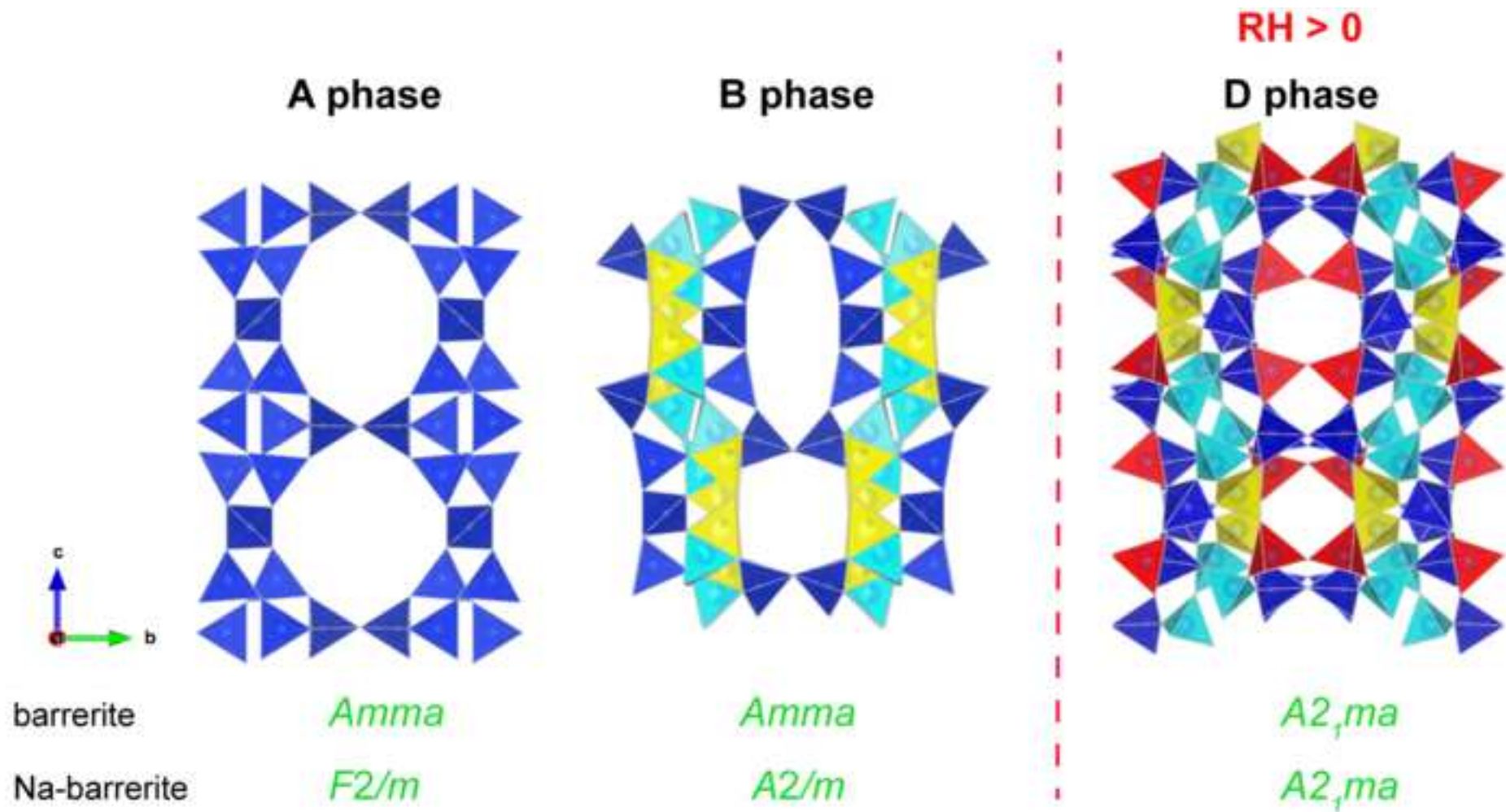


- Na-exchanged barrerite was found to be monoclinic ($F2/m$) similarly to stilbite
- D phase did not occur under dry ($RH = 0$) experimental conditions
- D phase of Na-exchanged barrerite was determined by *ex-situ* experiment
- A precursor model from B to D phase is suggested



Thermal Stability of Barrerite and Na-exchanged Barrerite: an *in situ* Single Crystal X-ray Diffraction Study Under Dry Conditions

Georgia Cametti^{a*}, Thomas Armbruster^a, Mariko Nagashima^b

^aMineralogical Crystallography, Institute of Geological Sciences, University of Bern Baltzerstr. 1+3, 3012 Bern, Switzerland

^bGraduate School of Science and Engineering, Yamaguchi University, Yamaguchi 753-8512, Japan

Abstract

The thermal stability of barrerite ($\text{Na}_{8.2}\text{K}_{3.0}\text{Ca}_{2.2}\text{Mg}_{0.2}\text{Al}_{17}\text{Si}_{55}\text{O}_{144}\cdot 50\text{H}_2\text{O}$) from Kuiu Island, Alaska, was investigated from 25°C to 500°C by *in situ* single-crystal X-ray diffraction under dry conditions. Corresponding experiments were performed on Na-exchanged barrerite $\text{Na}_{17}\text{Al}_{17}\text{Si}_{55}\text{O}_{144}\cdot 45\text{H}_2\text{O}$ from the same locality. The natural sample showed a gradual transformation of the A phase with dehydration to the B phase associated with rupture of T-O-T links and formation of new connections. Though, the high temperature modification (phase D) was not observed in the studied temperature range. In contrast to natural barrerite (space group *Amma*), Na-exchanged barrerite was found to be monoclinic *F2/m* at room temperature and transformed to *A2/m* (same cell setting) with beginning dehydration at 50°C. Its dehydration trend, monitored by unit-cell volume, corresponded to structural modifications observed for natural barrerite. The D phase of this sample was produced by *ex situ* experiments at 525°C under ambient conditions. A new model for transformation from the disordered B phase to the ordered highly condensed D phase (space group *A2₁ma*) is presented. In addition, the new *in situ* equilibrated single-crystal experiments are compared with dynamic X-ray powder diffraction studies.

Keywords: barrerite, dehydration, Na-exchanged barrerite, **STI** framework-type, zeolite

*corresponding author: georgia.cametti@krist.unibe.ch

1. Introduction

Barrerite with idealized chemical formula $\text{Na}_{16}\text{Al}_{16}\text{Si}_{56}\text{O}_{144}\cdot 52\text{H}_2\text{O}$ ($a = 13.2$, $b = 18.6$, $c = 17.8$ Å, space group *Amma*) is a natural zeolite [1] of stilbite framework-type (**STI**) [2]. Its structure is built by $4^2 5^4$ secondary building units (SBUs) and consists of 10-membered ring channels along the **a**-axis and 8-membered ring channels along the **c**-axis. Na ions and H_2O molecules are the most abundant extraframework (EF) occupants that are disorderly distributed at partially occupied sites [3, 4]. Barrerite shares the same framework topology with other two zeolite minerals, stellerite $\text{Ca}_8\text{Al}_{16}\text{Si}_{56}\text{O}_{144}\cdot 58\text{H}_2\text{O}$ and stilbite $\text{Na}_2\text{Ca}_8\text{Al}_{18}\text{Si}_{54}\text{O}_{144}\cdot 60\text{H}_2\text{O}$. The different symmetry of these three minerals is controlled by the EF cations and their distribution within the zeolitic channels. Thus, stellerite adopts the highest symmetry (*Fmmm*) [5, 6, 7], stilbite the lowest (*F2/m*) [8, 9, 10, 11] and barrerite is orthorhombic *Amma* [3, 4]. The distinct space groups observed in barrerite, stilbite, and stellerite are explained in terms of electrostatic repulsive forces between the extraframework cations [3, 5, 12].

According to ^{29}Si and ^{27}Al MAS-NMR studies the natural **STI** type zeolites show a disordered Si/Al distribution [13, 14, 15]. Based on ^{17}O triplequantum magic-angle spinning nuclear magnetic resonance (3QMAS NMR) natural stilbite contains even significant concentrations of Al-O-Al

linkages [16]. However, local Si/Al order was proposed for stilbite to explain small deviations from monoclinic symmetry [17]. Several stilbite crystals (from different localities) exhibit optical symmetry lower than that determined by X-ray diffraction [17]. This is explained by growth sectors of different symmetry. The relation between the orthorhombic and monoclinic sectors was interpreted by variable rotational order-disorder of framework tetrahedra occurring during crystal growth [17].

The exchange properties of stilbite, stellerite, and barrerite were investigated by Passaglia (1980) [18] and the role of the exchangeable cations on the heating behavior was explored. Crystal chemical and structural studies [19, 3, 5] demonstrated that repulsive action of the Na ions is responsible for the reduction of symmetry. Stellerite and barrerite show almost the same Si/Al ratio, therefore stellerite (*Fmmm*) crystals that were exchanged with Na ions should transform to space group *Amma* (the space group of barrerite). However, this assumption was not confirmed by the structural analysis of a completely Na-exchanged stellerite sample, which maintained the original *Fmmm* symmetry [20]. ND₄⁻ and NH₄⁺-exchanged forms of barrerite adopt the same symmetry of stellerite, *Fmmm* [21, 22]. Similarly, when barrerite crystals are completely exchanged with Ca, the topological *Fmmm* symmetry resulted [23].

The dehydration behavior of barrerite was investigated by X-ray diffraction techniques and mainly described as a two-step process: transformation from phase A to phase B at ca. 250°C and additional structural change to phase D at ca. 450-500°C [24, 25, 26]. The modifications, which barrerite undergoes upon heating, involve the statistical breaking of one T-O-T bridge that gives rise to two half-occupied face-sharing tetrahedra in phase B [24]. Interrupted T-O-T connection may be partially compensated by terminating T-OH groups [27]. The D phase is characterized by an additional volume contraction (ca. 20% compared to the RT value), by lower space group symmetry *A2₁ma*, and a new type of framework topology [25]. Stilbite and stellerite show similar trends upon heating [6, 11] but in contrast to barrerite the high temperature D phase does not form. With increase of temperature these structures collapse and turn X-ray amorphous [7].

In this study we investigated the dehydration process of a natural sample of barrerite by *in-situ* single crystal X-ray diffraction under dry conditions. In addition, a crystal belonging to the same sample was exchanged with NaCl solution in order to obtain a pure Na endmember of barrerite (Na-barrerite), on which another set of X-ray experiments was performed from RT to 450°C. Our aim is to compare these new results with those obtained by in situ synchrotron X-ray powder diffraction (XRPD) [26] and to determine whether differences occur in dehydration behavior of endmember Na-barrerite.

2. Experimental methods

2.1 Chemical analyses

The sample of barrerite used in the present study is from Rocky Pass, Kuiu Island, Alaska (sample number 43186 of Natural History Museum of Bern) [28]. The chemical composition was determined by electron-microprobe analyses (EMPA) by using a JEOL JXA-8230 instrument (installed at the Yamaguchi University) with the following analytical conditions: excitation voltage 15 KV, beam current 2 nA, beam diameter 10 µm. The standards were: wollastonite (Si *Kα* and Ca *Kα*), corundum (Al *Kα*), albite (Na *Kα*), rutile (Ti *Kα*), eskolaite (Cr *Kα*), Ca₃(VO₄)₂ (V *Kα*), hematite (Fe *Kα*), manganosite (Mn *Kα*), periclase (Mg *Kα*), K-feldspar (K *Kα*), SrBaNb₄O₁₂ (Sr *Lα* and Ba *Lα*), NiO (Ni *Kα*), KTiOPO₄ (P *Kα*), fluorite (F *Kα*), halite (Cl *Kα*). The ZAF (atomic number -absorption - fluorescence) correction-method [29] was used for all elements.

2.2 Cation exchange

In order to obtain a pure Na endmember of barrerite additional crystals of barrerite with dimension ranging from 0.10 to 0.50 mm were placed in a Teflon lined autoclave filled with 2 M NaCl solution for 2 weeks at 100(5)°C. The NaCl solution was renewed every three days. The Na-exchanged barrerite was qualitatively analyzed by a scanning electron microscope (SEM).

2.3 Single crystal X-ray diffraction

The crystal structure of barrerite was investigated by single-crystal X-ray diffraction (SCXRD) using a BRUKER APEXII diffractometer with a MoK α radiation ($\lambda = 0.71073$ Å) and a CCD area detector. The selected crystal (size ca. 0.35 x 0.40 x 0.25 mm) was glued on the tip of a glass fiber mounted on a goniometer head. The dehydration process was investigated from RT to 500°C using a self-constructed temperature controlled N₂-blower. The temperature was increased in steps of 25°C and before starting the data collection the sample was let equilibrated for ca. 40 minutes. Under these experimental conditions the crystal was continuously exposed to a dry N₂ atmosphere (RH = 0). Each data collection lasted ca. 8 hours. The data were integrated and an empirical absorption correction was applied using the Apex 2v. 2011.4-1 software package. Structures were solved using Shelxtl-2008 [30].

Structural refinements were carried out by SHELXL-2014 [31], using neutral atomic scattering factors.

The structure of barrerite at room temperature (phase A) was solved in space group *Cmcm*, transformed in *Amma* according to Galli and Alberti [3]. Atomic coordinates and labels of the framework were those adopted from Sacerdoti et al. [4]. The extra-framework occupants, both cations and H₂O molecules, were located by exploring difference-Fourier maps. The positions were assigned on the basis of the cation to oxygen framework distances and taking into account the chemical composition. Nevertheless, discrepancy between calculated and refined chemical composition occurs due to partial occupancy and closely spaced disordered sites.

Amma space group was maintained in the whole temperature range. Labels of atomic coordinates of the framework from 150°C to 500°C were those used by Ori et al. [26]. Extra-framework occupants were renamed because no correspondence was found with reference data [26]. In all data sets, framework sites were refined anisotropically whereas, in general, atomic displacement parameters of EF cations and H₂O sites were kept isotropic (exceptions are indicated in Tables). At 250°C the O3 site showed positional disorder and was split in two subsites, O3 and O3A, 0.58(3) Å apart.

A second set of X-ray diffraction experiments were performed on a Na-exchanged single crystal of barrerite with dimension of approximately 0.35 x 0.20 x 0.20 mm. The dehydration behavior of this sample was investigated from RT to 450°C applying the same experimental set-up used before. Structure solution at room temperature indicated monoclinic symmetry *C2/m*, transformed to the non-standard setting *F2/m* [32] to allow a direct comparison of cell dimension of **STI** type structures. Atomic coordinates and labels of framework sites were those of stilbite reported in [32]. For easy comparison with the RT data set structural data obtained from 50°C to 450°C were transformed to *A2/m* setting with corresponding axial orientations as for space group *F2/m* (Table 2). Pseudomerohedral twinning (matrix: [100 010 00-1], twin fraction ca. 0.12/0.88) was observed for all data sets. Additional refinement details are summarized in the supplementary material (SM1).

Another Na-exchanged crystal (size ca. 0.20 x 0.10 x 0.15 mm) of barrerite was heated *ex situ* at 525°C in order to investigate a possible transformation to the D phase reported for natural barrerite. Under this experimental conditions the sample was not exposed to dry conditions but heated in air. The crystal was gradually heated (65°C/h) up to 525°C. This temperature was kept for ca. 4 h and then the crystal was let cool down for ca. 2 h before starting the data collection. The structure was solved in space group *A2₁ma* [25] and atomic coordinates and labels by Sacerdoti [25] were used. Crystal data and refinement parameters are reported in Table 1a,b.

3. Results

The crystal-chemical formula of natural barrerite calculated according to chemical analyses is $\text{Na}_{8.24}\text{K}_{3.04}\text{Ca}_{2.24}\text{Mg}_{0.24}\text{Al}_{16.8}\text{Si}_{54.96}\text{O}_{144} \cdot 50\text{H}_2\text{O}$ (Table 3). Coordinates of this barrerite structure at room temperature and corresponding bond-length distances are reported in Tables S1 and S2, respectively. Structural data for natural barrerite at 150 and 275°C are shown in Table S3 and S4. Table 4 displays structure parameters of Na-exchanged barrerite at room temperature. Results of structure refinements of the B-phase at 150°C and at 350°C are summarized in Tables S5 and S6, respectively, and those of the *ex-situ* D-phase (produced at 525°C) in Table S8. Table S7 summarizes the relation between labels of tetrahedral sites in different barrerite structures. CIF files have been submitted as supplementary material.

3.1 Natural barrerite

The structure at room temperature of natural barrerite was found to be in agreement with previously reported results [3, 4]. The main difference is related to the location of the EF cations that in our study are distributed over 9 partially occupied crystallographic sites (Table S1, S2). Sacerdoti et al. [4] refined a sample from the same locality with 5 independent sites. H_2O molecules were located on 21 partially occupied sites in contrast to 14 sites found by Sacerdoti et al. [4].

The dehydration process started at 50°C and proceeded up to 275°C. In this temperature range the transition from the A to the B phase was observed and the unit-cell volume decreased from 4409.8(3) Å³ at 25°C to 3738.66(15) Å³ at 275°C (Fig.1). This reduction of volume was accompanied by the total loss of the original water content (55.6 H_2O) at 275°C. The structural transformations affecting barrerite in this first dehydration step mainly involved the rotation of the SBUs leading to a more elliptical shape of the channel cross-sections (Fig. 2). At 150°C new electron-density peaks appeared in difference Fourier maps close to oxygen-framework atoms of the triangular basis of the SiO_4 tetrahedra (Table S3). These peaks corresponded to low-occupied new tetrahedral Si, Al sites occurring as a consequence of the T-O-T breaking. At 200°C, in addition to the new T centers, a new oxygen site (OD) was found representing the alternate tetrahedral apex linking the new T1D and T4D tetrahedra. The occupancy of these new sites progressively increased with temperature while the occupancy of the original sites decreased until at 275°C both were half occupied and the B phase reported by Alberti and Vezzalini [24] was obtained (Table S4). This process has to be regarded as a gradual transition from the *Amma* room temperature structure to the *Amma* contracted B phase at 275°C, during which Si, Al atoms migrated toward the new positions in a disordered fashion.

At 300°C the so called face-sharing tetrahedra remained half occupied by Si, Al. Upon further heating up to 500°C the structure did not undergo additional significant modification preserving space group *Amma*. Transformation to the D phase was not observed.

3.2 Na-barrerite

Complete Na-exchange was confirmed (absence of Ca and K) by qualitative energy dispersive analysis using a scanning electron microscope (SEM). The crystal structure of the Na-barrerite sample at room temperature was solved and successfully refined in the monoclinic space group *F2/m* (Table 4), similar to the structure of the stilbite. The monoclinic angle, $\beta = 90.429(1)^\circ$, is close to that reported for natural stilbite [8, 9]. The **STI** type framework-topology is maintained but the symmetry lowered to monoclinic (Fig. 3). The investigated sample showed a strong orthorhombic pseudo-symmetry *Cmcm* (*Amma*). However, we tested different crystals and all the data sets exhibited an angle $\beta = 90.2\text{--}90.5^\circ$. The data were collected with high redundancy (8 for orthorhombic and 4 for monoclinic) and in orthorhombic symmetry the final R_{int} (0.0796) value was larger than R_σ (0.0531),

whereas in monoclinic R_{int} (0.0501) was similar to R_e (0.0569). This discrepancy became enhanced at higher temperatures.

Moreover, choice of *Amma* symmetry (for test purposes) at elevated temperature indicated few significant systematic absence violations (*a* glide) and more important an extended list of inconsistent equivalent F_{obs} values. Corresponding discrepancies were not seen in monoclinic refinements.

The dehydration behavior proceeded via a similar trend as observed for the natural sample. As shown in Figure 1 the decrease of the unit-cell volume (from $V = 4407.12(14) \text{ \AA}^3$ at RT to $V = 3742.42(17) \text{ \AA}^3$ at 450°C) upon heating and the associated release of water was very similar for both barrerite samples. Nevertheless, as soon as the dehydration started at 50°C the structure of the Na-barrerite changed Bravais centering from $F2/m$ to $A2/m$ with corresponding cell setting and volume. The $A2/m$ space group was preserved up to 450°C . The gradual transformation to the B phase accompanied by formation of disordered “face-sharing” tetrahedra started at 150°C at which the monoclinic B phase is characterized by rupture of two T-O-T connections, T1M-O3-T4M and T4-O5-T2, though related by pseudo-symmetry (Table S5). Surprisingly, the occupancies of the new T sites (T1MD, T4MD connected by OD2 and T4D, T2D connected by OD1) converged at 350°C to 1/3 and 2/3, respectively (Table S6) and not to 1/2 each, determined for natural barrerite. This uneven ratio remained unchanged up to the maximum temperature of 450°C . The new connections T1MD-OD2-T4MD and T4D-OD1-T2D in the B phase of Na-barrerite ($A2/m$) correspond topologically to T1D-OD-T4D in the B phase of natural barrerite in space group *Amma* (S7). Thus, averaged over the Na-barrerite ($A2/m$) B phase structure the number of new T-O-T connections is the same as in natural barrerite. The uneven ratio of new T-O-T connections in Na-barrerite is also the reason that with increasing temperature the difference to orthorhombic diffraction symmetry becomes more pronounced.

3.2.1 Na-barrerite phase D

Our *ex situ* experiment demonstrated that the monoclinic Na-barrerite transforms to a highly-condensed orthorhombic ordered D phase (space group $A2_1ma$, $a = 12.955(4)$, $b = 16.850(5)$, $c = 16.236(5) \text{ \AA}$, $V = 3544.3(18) \text{ \AA}^3$) without microporous character in contrast to the B phase (Fig. 4). The structure (Table S8) corresponds to that reported by Sacerdoti [25] for a natural sample of barrerite. The total decrease of the unit-cell volume is 20% with respect to the fully hydrated sample measured at room temperature.

4. Discussion

4.1 Comparison with synchrotron XRPD

In general, the structural transformations of natural barrerite found in our experiments correspond to those previously reported [24, 25, 26]. However, comparing our results with the dynamic *in situ* dehydration study performed by Ori *et al.* [26] differences are observed. In the powder diffraction experiments the authors reported that the percentage of broken T-O-T bridges begins at 250°C and remains unchanged with temperature. In our study, the change from A to B phase of barrerite is described by a gradual transition due to progressive rupture of the T-O-T bridges. The percentage of broken T-O-T bridges increases as a function of temperature from 150°C to 275°C until it reaches 50%. Only after this value is achieved the occupancy of T sites remains unvaried up to 500°C .

The different kinetics, due to experimental set-up, resulted in our data a shift of the structural transformations toward lower temperatures compared to XRPD experiments (Fig. 1). This is a well-known effect [33, 34] that non-equilibrium experiments (XRPD) show a larger unit cell associated to the dehydration steps compared to equilibrated experiments (SCXRD). Surprisingly, the trend is inverted above 300°C . The volume change observed in our experiments reaches a plateau above

275°C and it does not vary significantly afterward. At 500°C the B phase is still preserved and barrerite does not transform to the D phase. In contrast to our single-crystal results, the XRPD experiments show in the range from ca. 340 to 470°C, at which only the B phase is analyzed, a gradual decrease of the unit-cell volume. Then the volume rapidly decreases because of the strong contraction characteristic of the D phase.

The different volume trend observed in our experiments and the fact that heating effects are shifted to lower temperatures with the exception of formation of the D phase, may be interpreted in terms of the dynamic nature of the XRPD experiments and the different EF cation content of our sample compared to the one used in Ori et al. [26], typical of natural samples. The transformation from A to B phase is mainly related to the strain induced on the O framework by the EF cations to achieve more energetically balanced coordination after the release of water. In contrast, the subsequent phase transition from B to D is not related to loss of H₂O (barrerite above 275°C is in our experiments anhydrous). The D phase, as discussed below, involves a severe readjustment of the framework tetrahedra that may be influenced by locally ordered Si/Al distribution [17]. Another factor that at this stage becomes important, is the small size of grains in powder material compared to our single crystal (ca. 0.3 mm). A faster reaction is expected as a consequence of the short diffusion-path in powder compared to single crystal. A more convincing interpretation of the constant volume observed in our experiments between 275 and 500°C is suggested by considering the following section.

4.2 The role of $RH = 0$ and T-OH termination on the formation of D phase

Alberti et al. [27] provided convincing evidence by *near infrared* (NIR) diffuse reflectance spectra that the B, C (rehydrated B phase), and the D phase display absorptions at ca. 2200 nm (4550 cm⁻¹) interpreted as ν_{OH} and δ_{SiOH} combination bands due to OH groups. These absorptions did not occur in phase A barrerite and are characteristic of zeolite structures with broken T-O-T connections investigated under ambient conditions [35, 36]. In test refinements we controlled the occupancies of the new occurring and original T sites without any constraints. Our results did not indicate significant deviations of equal occupancies of pairs for T sites involved in formation of new T-O-T connections. This result is also corroborated by the independently refined atomic displacement parameters of these sites, which converged to very similar values. The same test (refinement without constraints) was performed on the oxygen site of the new tetrahedral apex (OD). The refined occupancy and values of atomic displacement parameters confirmed that the OD site is always shared by the two tetrahedral sites (T1D and T4D), excluding significant T-OH groups in our B phase. Thus, the dry conditions in our experiments may even have prevented formation of terminating T-OH groups.

An interesting conclusion can be drawn concerning this point. If OH groups do not form under our experimental conditions, the B phase that we observed is actually different from that analyzed under ambient conditions (mainly relative humidity higher than 0) in previous studies [24, 27]. Assuming that the D phase arises only as a consequence of the function and subsequent loss of OH groups from B phase [24], our dry conditions also explain why we did not observe the D phase up to 500°C in the *in situ* experiments. The idea that our B phase is not hydroxylated is also supported by the constant volume observed from 275 to 500°C (Fig. 1). Curing of T-OH terminations to T-O-T connections would lead to increasing condensation associated with a decrease of volume.

The D phase [25] does not contain OH groups or at least, if it does, only in very low concentration below the resolution of the single-crystal experiment. The OH-bearing barrerite D phase in Alberti et al. [27] was obtained after heating the crystal at 398°C and it may correspond to a T-OH containing precursor of the real phase D.

Finally, the percentage of T-OH terminations reported in Alberti et al. [27] is probably overestimated; Ori et al. [26] did not report (and even mention) evidence of significant OH terminations that are probably under the detection limit of the XRPD technique (SFig. 1).

Interestingly, powder data on stilbite phase B also indicated a small percentage of T-OH terminations [11], whereas the structure of stellerite B is even characterized by dominating T-OH with less new T-O-T connections leading to an interrupted framework [7]. The framework structure of stellerite B [6] is topologically equivalent to that of barrerite, whereas the one of stilbite B [11] is different because different T-O-T connections are broken.

4.3 Formation of the D phase: a hypothetical precursor phase

The reinvestigation of the D phase suggested a different idealized B phase, as a precursor model, compared to that previously reported [25]. In the latter model, complete migration from original to new tetrahedral sites is assumed whereas in our model 50% of each new (T1D and T4D) and original (T1 and T4) T sites are arranged in an ordered fashion. Thus, the transformation from the B phase to the precursor structure of the D phase represents a disorder-order transition. In the observed condensed D phase, strain release causes additional rupture of T-O-T bonds (T1-O1-T4) associated with new T-O-T (T1D-OD-T4D) connections.

The D phase arises from the rearrangement of the B phase framework through two main processes. In the B phase, T atoms are randomly distributed at the original tetrahedral sites (corresponding to those fully occupied in the A phase) and at new ones formed as a consequence of the T-O-T rupture. In addition, T-OH terminations are statistically replacing T-O-T connections in the B structure [27]. Partial curing of such terminated T-OH units in favor of new T-O-T links may be the cause of the initial volume decrease observed between 340 and 470°C in XRPD data [26]. The first step requires a transition from the disordered tetrahedral framework of the B phase to an ordered orthorhombic precursor structure of the D phase. This ordering process is catalyzed by OH groups. The resulting precursor phase is assumed to have 50% of the new tetrahedra and 50% of the original tetrahedra fully occupied in an ordered fashion (Fig. 5a,b). In a second step, this precursor phase transforms to the D phase when additional tetrahedra flip inside the 8-ring channels forming new linkages. Thus the channels become occluded and the new condensed structure (Fig. 5c) loses microporous properties. If the T-OH terminations [27] either not form or are very scarce under dry conditions (our experiments), the ordering process of the disordered B phase to the ordered precursor phase is hampered and the D phase does not form in the investigated temperature range.

For Na-barrerite, formation of the D phase was only observed *ex situ* at 525°C under ambient humidity conditions in the furnace. The observation that in the Na-barrerite B phase, produced under dry conditions, unequal numbers of new T-O-T connections are formed and not ½ as required for the D phase is additional support that formation of the D phase under dry conditions is hampered.

4.4 Considerations on the memory effect of the **STI** framework type

Our results demonstrate the sensitivity of the **STI** framework-type to the content of EF cations. If the symmetry of a **STI** framework-type mineral is only governed by the EF cations and the associated H₂O molecules, Na-exchanged end-members of stellerite, stilbite, and barrerite should be symmetrically identical. Otherwise a memory effect (e.g. by slightly different Si, Al distributions) of the framework must be considered as origin of different symmetry of Na-exchanged members.

Passaglia and Sacerdoti [20] investigated a completely Na-exchanged stellerite, demonstrating that the framework preserved the space group *Fmmm* of the original stellerite crystal and did not adopt *Amma* symmetry assumed for barrerite. At the first glance this finding would support existence of a framework memory-effect. However, our new results showing *F2/m* symmetry for Na-exchanged barrerite offer a different interpretation. Due to the topological *Fmmm* symmetry of the **STI** framework type, differences between *Fmmm* and *F2/m* are difficult to resolve if the β angle is very close to 90°. In our study, the difference between *Fmmm* and *F2/m* symmetry became mainly apparent

after collecting intensity data with high redundancy. Based on the internal agreement factors of symmetry equivalent reflections, the intensity distribution is in agreement with $F2/m$ but not with $Fmmm$ symmetry. Passaglia and Sacerdoti [20] essentially collected a unique data set for F -centered orthorhombic setting as customary for diffractometers equipped with a point counter about 35 years ago. We suppose that with the limited data they could not detect the lower symmetry. In addition, their main intention was to demonstrate that the F -centered lattice was in contrast to A -centering expected by them. This also confirmed by our structure refinements on Na-barrerite at RT.

Na-exchanged stilbite [37] showed an X-ray diffraction powder-pattern similar to stilbite ($F2/m$) but the symmetry was not thoroughly investigated. Synthetic barrerite [38] produced an X-ray powder pattern, which was only qualitatively evaluated to be in agreement with natural barrerite ($Amma$). Thus none of the previous reports could provide a convincing answer on the true symmetry of the fully hydrated Na-endmember with **STI** framework type. We currently produce Na-exchanged stellerite crystals to test by new structure refinements whether assumption of the memory effect of the **STI** framework-type can be maintained.

Acknowledgements We are thankful to Beda Hofmann of Natural History Museum of Bern who kindly provided the barrerite sample and to Alfons Berger for assistance in SEM analyses. We also thank two anonymous reviewers for their helpful comments.

References

- [1] E. Passaglia, D. Pongiluppi, *Mineral. Mag.* 40 (1975) 208.
- [2] Ch. Baerlocher, W.M. Meier, D. H. Olson, Atlas of zeolite framework types, Structure commission of the IZA, Elsevier, 5th ed. 2001, 302p.
- [3] E. Galli, A. Alberti, *Bull. Soc. Fr. Mineral. Cr.* 98 (1975) 331-340.
- [4] M. Sacerdoti, A. Sani, G. Vezzalini, *Micropor. Mesopor. Mat.* 30 (1999) 103-109.
- [5] E. Galli, A. Alberti, *Bull. Soc. Fr. Mineral. Cr.* 98 (1975a) 11-18.
- [6] A. Alberti, R. Rinaldi, G. Vezzalini, *Phys. Chem. Miner.* 2 (1978) 365-375.
- [7] R. Arletti, E. Mazzucato, G. Vezzalini, *Am. Mineral.* 91 (2006) 628-634.
- [8] E. Galli, G. Gottardi, *Miner. Petrogr. Acta* 12 (1966) 1-10.
- [9] M. Slaughter, *Am. Mineral.* 55 (1970) 387-397.
- [10] W. J. Mortier, *Am. Mineral.* 68 (1983) 414-419.
- [11] G. Cruciani, G. Artioli, A. Gualtieri, K. Ståhl, J. C. Hanson, *Am. Mineral.* 82 (1997) 729-739.
- [12] E. Galli, *Acta Cryst.* B27 (1971) 833-841.
- [13] E. Lippmaa, M. Mägi, A. Samoson, M. Tarmark, G. Engelhardt, *J. Am. Chem. Soc.* 103 (1981) 4992-4996.
- [14] A. Sani, C. Marichal, C. Forte, *Plinius*, 22 (1999) 344-345.
- [15] A. Sani, L. Del Motte, C. Marichal, Z. Gabelica, C. Forte, *Eur. J. Mineral.* 13 (2001) 101-111.
- [16] J. F. Stebbins, P. Zhao, S. Keun Lee, X. Cheng, *Am. Mineral.* 84 (1999) 1680-1684.
- [17] M. Akizuki, H. Konno, *Am. Mineral.* 70 (1985) 814-821.
- [18] E. Passaglia, *Tscherm. Miner. Petrog. Mitt.* 27 (1980) 67-78.
- [19] E. Passaglia, E. Galli, L. Leoni, G. Rossi, *Bull. Mineral.* 101 (1978) 368-375.
- [20] E. Passaglia, M. Sacerdoti, *Bull. Mineral.* 105 (1982) 338-342.
- [21] E. Meneghinello, A. Alberti, G. Cruciani, M. Sacerdoti, G. Mc Intyre, P. Ciambelli, M. T. Rapacciuolo, *Eur. J. Mineral.* 12 (2000) 1123-1129.
- [22] A. Martucci, A. Alberti, M. Sacerdoti, G. Vezzalini, P. Ciambelli, M. Rapacciuolo, in: C. Colella, F. A. Mumpton (Eds.), Natural Zeolites for the Third Millennium, De Frede Editore, Napoli, 2000, p. 45.

- [23] M. Sacerdoti, I. Gomedì, *Bull. Mineral.* 107 (1984) 799-804.
- [24] A. Alberti, G. Vezzalini, in: L. B. Sand, J. Mumpton (Eds.), *Natural Zeolites. Occurrence, Properties, Use*, Pergamon Press, New York, 1978, pp. 85-98.
- [25] M. Sacerdoti, *Micropor. Mesopor. Mat.* 102 (2007) 299-303.
- [26] S. Ori, E. Mazzucato, G. Vezzalini, *Am. Mineral.* 94 (2009) 64-73.
- [27] A. Alberti, F. Cariati, L. Erre, P. Piu, G. Vezzalini, *Phys. Chem. Minerals*, 9 (1983) 189-191.
- [28] F. Di Renzo, Z. Gabelica, *Can. Mineral.* 35 (1997) 691-698.
- [29] J. L. Pouchou, F. Pichoir, in: *Microbeam Analysis 1988*, D. Newbury (Ed.), San Francisco Press, 319-324.
- [30] G. M. Sheldrick, *Acta Cryst.* A64 (2008) 112-122
- [31] G. M. Sheldrick, *Acta Cryst.* C71 (2015) 3-8.
- [32] S. Quartieri, G. Vezzalini, *Zeolites* 7 (1987) 163-170.
- [33] G. Cruciani, *J. Phys. Chem. Solids* 67 (2006) 1973-1994.
- [34] A. Martucci, E. Rodeghero, G. Cruciani, *Eur. J. Mineral.* 28 (2016) 5-13.
- [35] P. S. R. Prasad, K. S. Prasad, S. R. Murthy, *Am. Mineral.* 90 (2005) 1636-1640.
- [36] D. L. Bish, R. Milliken, C. T. Johnston, in: R. S. Bowman, S. E. Delap (Eds), *Zeolite '06-7th International Conference on the occurrence, Properties and Utilization of Natural Zeolites, Socorro, New Mexico USA, 16-21 July 2006*, pp. 53-54.
- [37] K. Harada, K. Tomita, *Am. Mineral.* 52 (1967) 1438-1450.
- [38] H. Ghobarkar, O. Schäf, U. Guth, *J. Solid State Chem.* 142 (1999) 451-454.

Figure(s)
[Click here to download high resolution image](#)

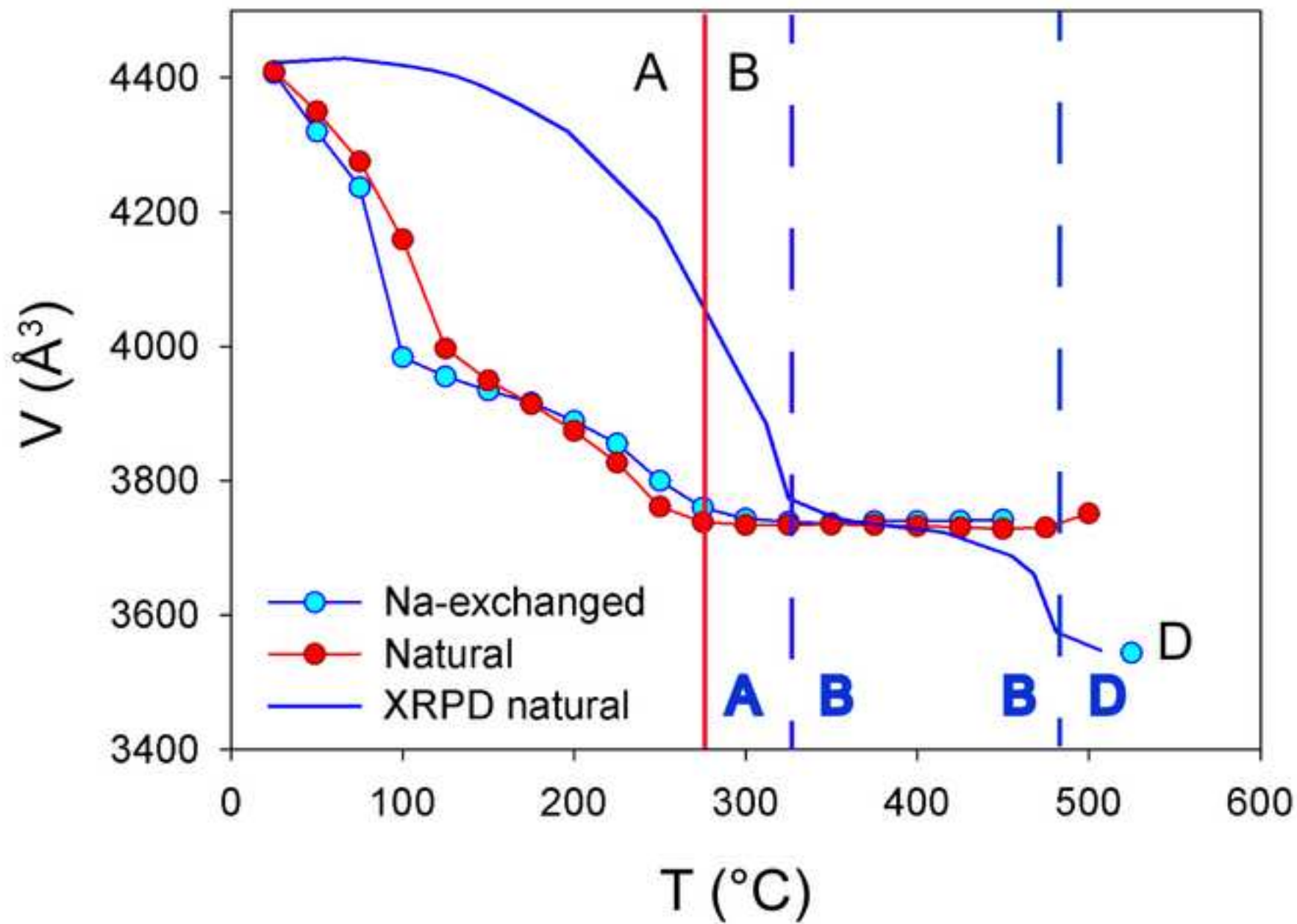


Figure 2
[Click here to download high resolution image](#)

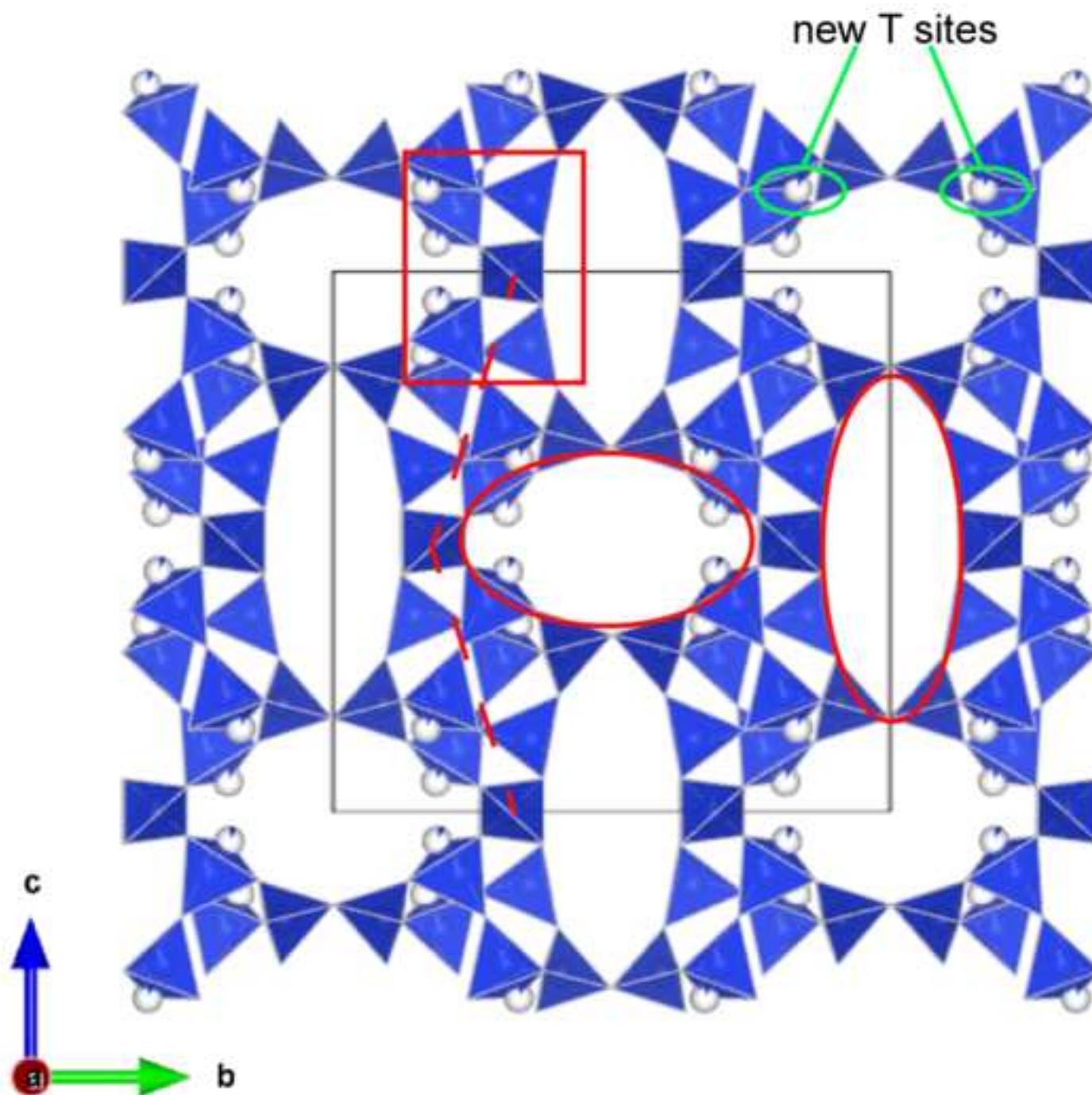


Figure 3
[Click here to download high resolution image](#)

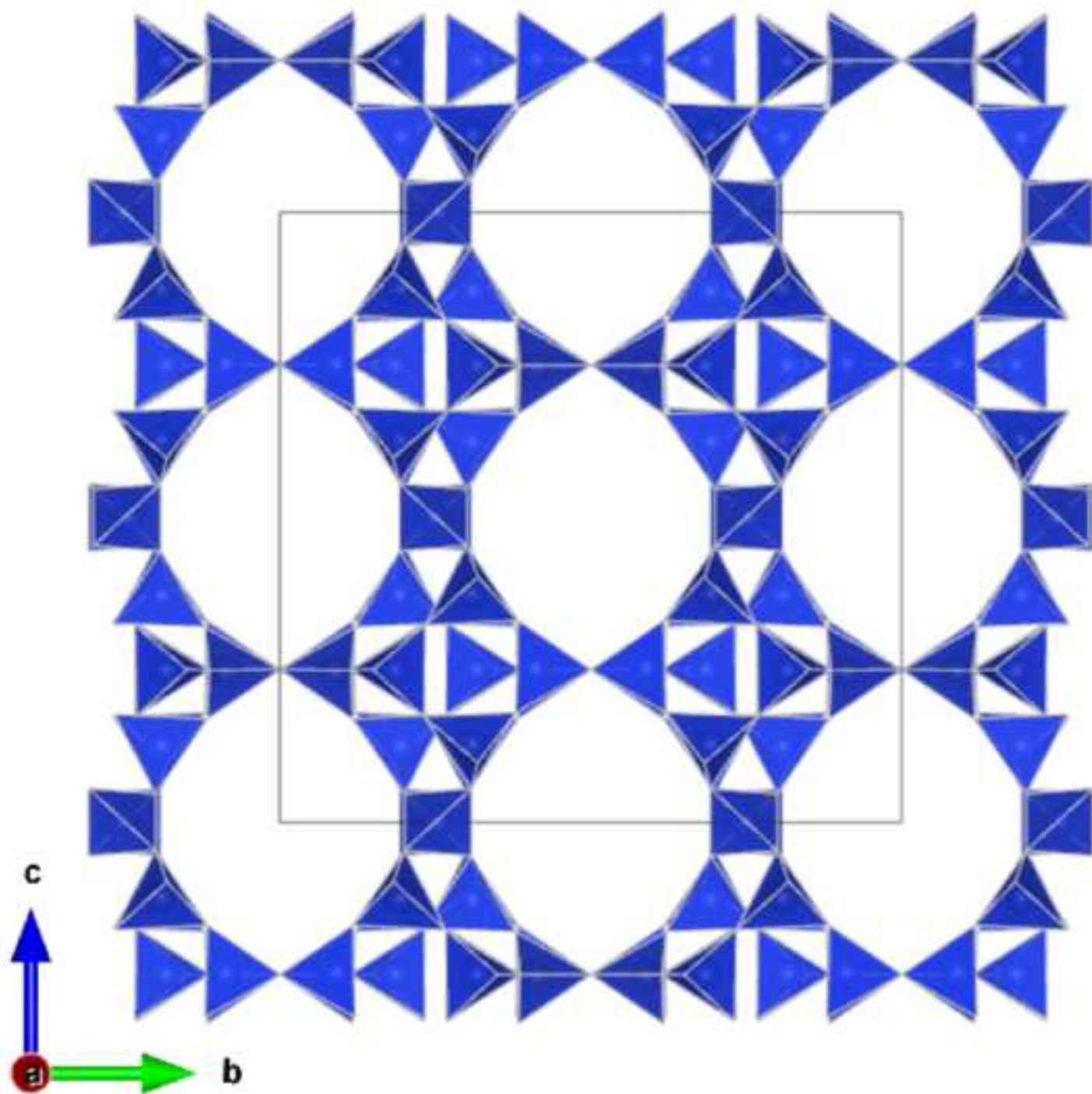
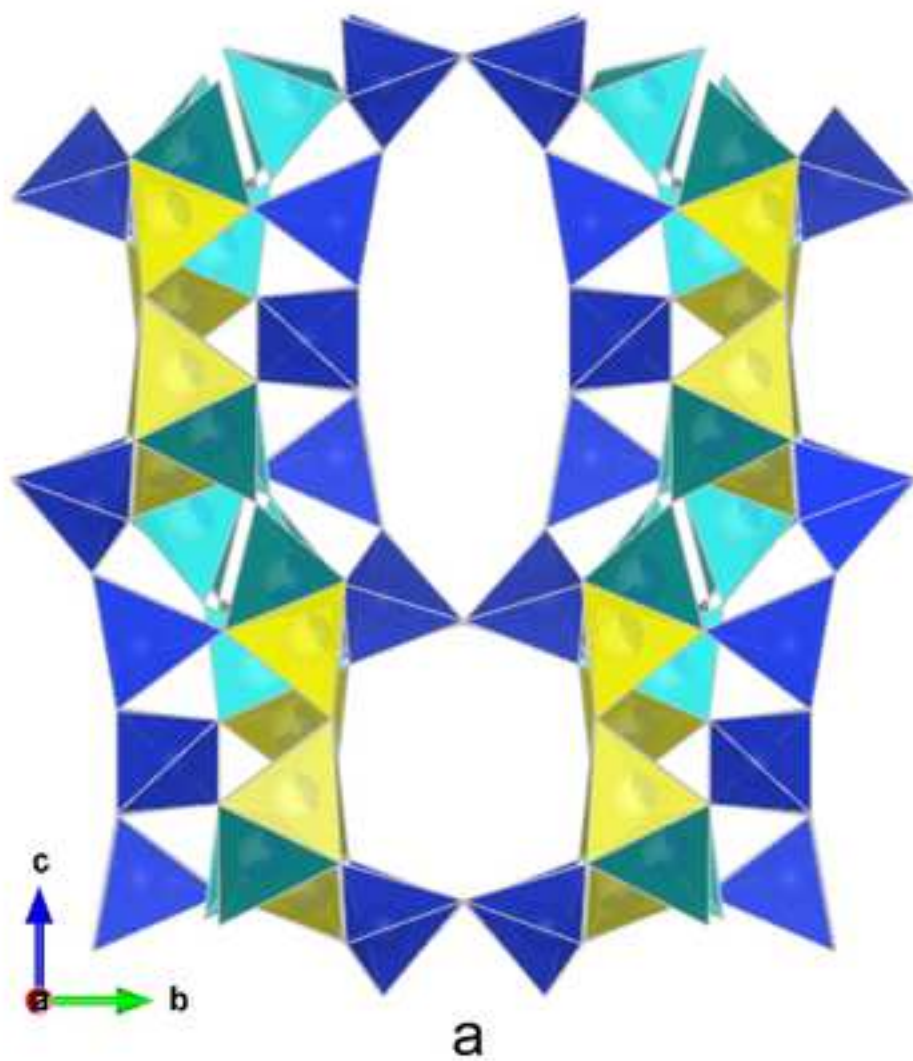


Figure 4
[Click here to download high resolution image](#)

B phase



D phase

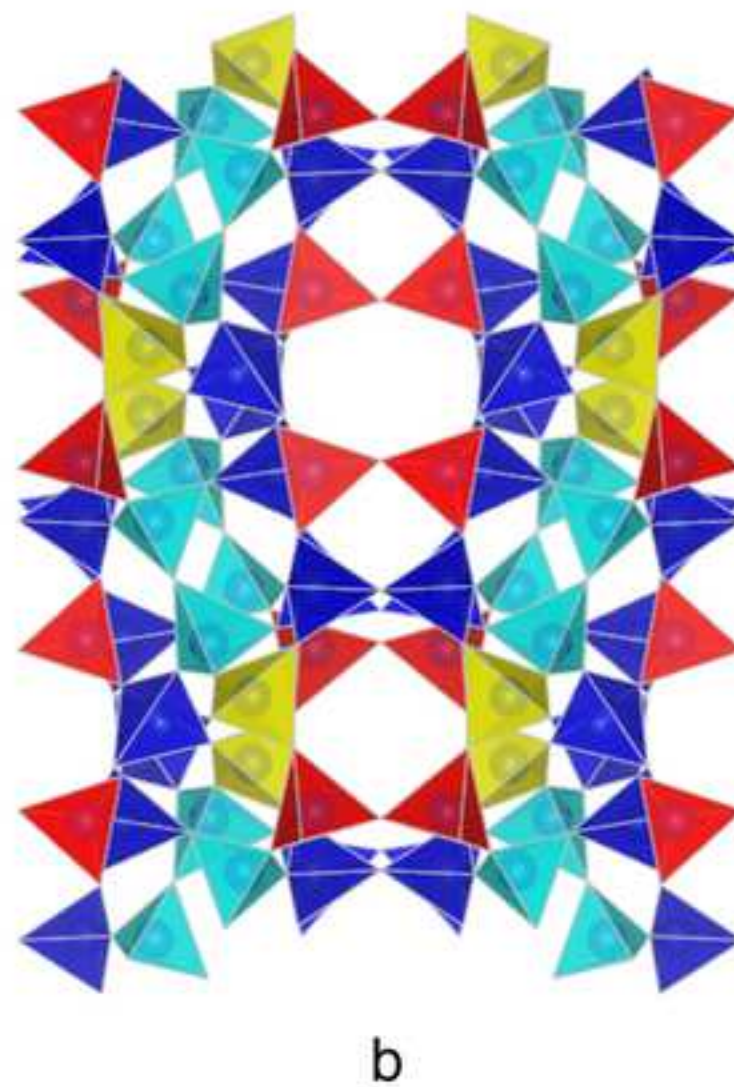
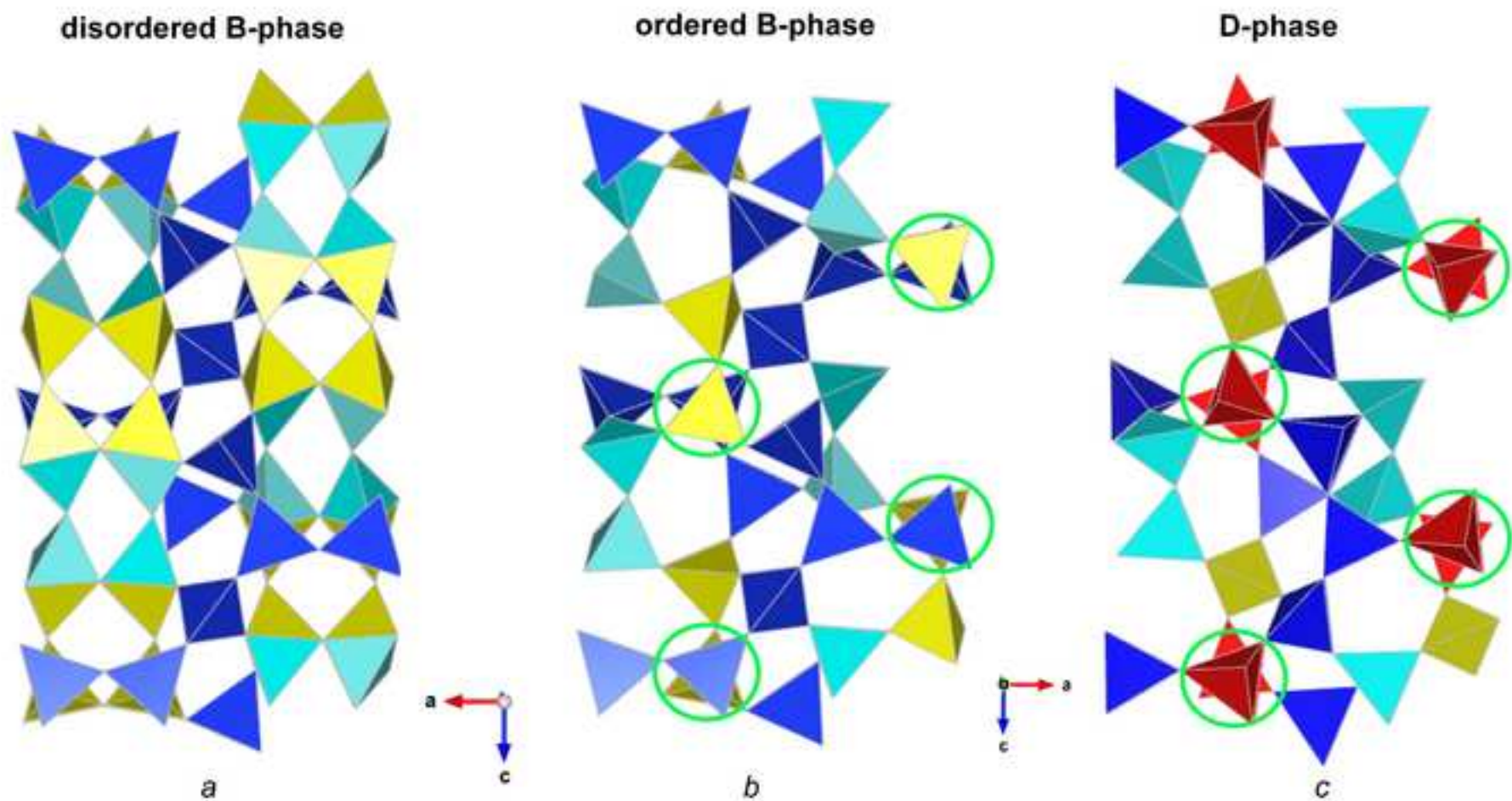


Figure 5
[Click here to download high resolution image](#)



Figures caption

Figure 1 Volume trend of natural (red dots) and Na-exchanged (light blue dots) barrerite as a function of temperature. Corresponding volume of Na-barrerite D phase (obtained *ex-situ* in air) is also shown. Synchrotron X-ray powder diffraction data (XRPD) are reported for comparison [25]. Vertical dotted blue lines at 325°C and 480°C represent the A-B and B-D transition as detected in XRPD reference data [25]. The vertical continuous red line at 275°C indicates the corresponding A-B transition in our dry experiments.

Figure 2 Tetrahedral framework of natural barrerite at 150°C. The deviation of subsequent $4^2 5^4$ secondary building units (SBUs) from the [001] direction is represented by the dotted line. Low-occupied new tetrahedral sites are shown as partially colored spheres. The elliptical shape of the channels is highlighted by red curves.

Figure 3 Framework of Na-exchanged barrerite at room temperature projected along [100] direction.

Figure 4 Phase B (a) and phase D (b) framework of Na-barrerite. Cyan (original T sites) and yellow (new T sites originated after the T-O-T rupture) polyhedra represent the statistically occupied face sharing tetrahedra associated with breaking of T-O-T bridges. The different occupancy ($\frac{2}{3}$ and $\frac{1}{3}$) of T sites in B phase is shown by dark and light colored (cyan and yellow) tetrahedra, respectively. Red tetrahedra correspond to those flipped inside the cages after the transformation to the condensed D phase.

Figure 5 Model of transformation from the disordered B phase to the orthorhombic ordered D phase. (a) Disordered B-phase at 350°C. Original (cyan) and new (yellow) tetrahedral sites are face-sharing and statistically occupied. (b) Hypothetic ordered B-phase; 50% of the original and 50% of the new T sites are fully occupied in an ordered-fashion. (c) condensed D-phase; apices of the red tetrahedra (in the circles) are reversed in viewing direction compared to (b) but the triangular basis is preserved.

Table 1a. Crystal data and refinement parameters for natural barrerite at room temperature (RT), 150°C (RH = 0), and 275°C (RH = 0).

Crystal data	Barrerite A RT	Barrerite A 150°C	Barrerite B 275°C
<i>a</i> -axis (Å)	13.6227(5)	13.6621(3)	13.6110(3)
<i>b</i> -axis (Å)	18.1780(7)	17.2677(4)	17.1485(4)
<i>c</i> -axis (Å)	17.8079(7)	16.7407(3)	16.0177(4)
Cell volume (Å ³)	4409.8(3)	3949.35(14)	3738.66(15)
Z	1	1	1
Space Group	<i>Amma</i>	<i>Amma</i>	<i>Amma</i>
Refined chemical formula	Na _{11.2} K _{1.16} Ca _{2.03} (Si,Al) ₇₂ O ₁₄₄ ·55.6H ₂ O	Na _{6.16} K _{1.30} Ca _{1.68} (Si,Al) ₇₂ O ₁₄₄ ·9H ₂ O	Na _{8.97} K _{1.30} Ca _{1.18} (Si,Al) ₇₂ O ₁₄₄
Intensity measurement			
Diffractionmeter		APEX II SMART	
X-ray radiation		MoK α λ =0.71073 Å	
X-ray power		50 kV, 30 mA	
Monochromator		Graphite	
Temperature (°C)	25	150	275
Time per frame	60	60	60
Max. 2 θ	84.21°	87.44°	77.13°
Index ranges	-25 ≤ <i>h</i> ≤ 25 -34 ≤ <i>k</i> ≤ 34 -33 ≤ <i>l</i> ≤ 33	-26 ≤ <i>h</i> ≤ 26 -33 ≤ <i>k</i> ≤ 33 -31 ≤ <i>l</i> ≤ 32	-23 ≤ <i>h</i> ≤ 23 -30 ≤ <i>k</i> ≤ 30 -28 ≤ <i>l</i> ≤ 27
No. of measured reflections	69973	56782	48914
No. of unique reflections	8153	7911	5595
No. of observed reflections <i>I</i> > 2 σ (<i>I</i>)	6038	5158	4141
Structure refinement			
No. of parameters used in the refinement	255	198	192
<i>R</i> (int)	0.0378	0.0438	0.0421
<i>R</i> (σ)	0.0250	0.0299	0.0239
GooF	1.065	1.057	1.089
<i>R</i> 1, <i>I</i> > 2 σ (<i>I</i>)	0.0445	0.0535	0.0556
<i>R</i> 1, all data	0.0624	0.0823	0.0744
w <i>R</i> 2 (on <i>F</i> ²)	0.1490	0.1954	0.1862
$\Delta\rho_{min}$ (eÅ ⁻³) close to	-0.80 from W7	-1.56 C2	-0.67 C2
$\Delta\rho_{max}$ (eÅ ⁻³) close to	0.97 from W7	1.02 C5	1.22 CW4

Table 1b. Crystal data and refinement parameters for Na-exchanged barrerite at room temperature (RT), 150°C (RH = 0), 150°C (RH = 0), and produced at 525°C (measured at RT).

Crystal data	Na-Barrerite A RT	Na-Barrerite B 150°C	Na-Barrerite B 350°C	Na-Barrerite D 525°C
<i>a</i> -axis (Å)	13.6288(2)	13.6703(2)	13.6132(10)	12.955(4)
<i>b</i> -axis (Å)	18.1600(3)	17.2196(3)	17.1442(13)	16.850(5)
<i>c</i> -axis (Å)	17.8071(4)	16.7145(3)	16.0105(13)	16.236(5)
β (°)	90.4290(10)	90.2750(10)	90.229(5)	90
Cell volume (Å ³)	4407.12(14)	3934.50(11)	3736.6(5)	3544.3(18)
Z	2	2	2	2
Space Group	<i>F</i> 2/ <i>m</i>	<i>A</i> 2/ <i>m</i>	<i>A</i> 2/ <i>m</i>	<i>A</i> 2 ₁ <i>ma</i>
Refined chemical formula	Na _{16.35} (Si,Al) ₇₂ O ₁₄₄ ·45.4H ₂ O	Na _{12.7} (Si, Al) ₇₂ O ₁₄₄ ·8.5H ₂ O	Na _{12.83} (Si, Al) ₇₂ O ₁₄₄	Na ₁₀ (Al,Si) ₇₂ O ₁₄₄
Intensity measurement				
Diffractionmeter		APEX II SMART		
X-ray radiation		MoKα λ=0.71073 Å		
X-ray power		50 kV, 30 mA		
Monochromator		Graphite		
Temperature (°C)	25	150	350	525
Time per frame	60	60	60	60
Max. 2θ	77.14°	64.45°	62.67°	34.60°
Index ranges	-23 ≤ <i>h</i> ≤ 23 -31 ≤ <i>k</i> ≤ 31 -31 ≤ <i>l</i> ≤ 30	-20 ≤ <i>h</i> ≤ 20 -25 ≤ <i>k</i> ≤ 25 -24 ≤ <i>l</i> ≤ 24	-19 ≤ <i>h</i> ≤ 19 -25 ≤ <i>k</i> ≤ 25 -23 ≤ <i>l</i> ≤ 22	-9 ≤ <i>h</i> ≤ 10 -13 ≤ <i>k</i> ≤ 14 -10 ≤ <i>l</i> ≤ 13
No. of measured reflections	27488	31207	23806	2310
No. of unique reflections	5092	6940	5862	932
No. of observed reflections <i>I</i> > 2σ (<i>I</i>)	3541	4995	4281	677
Structure refinement				
No. of parameters used in the refinement	207	357	342	133
<i>R</i> (int)	0.0501	0.0574	0.0524	0.1226
<i>R</i> (σ)	0.0569	0.0438	0.0423	0.1249
GooF	0.956	1.031	1.048	1.103
<i>R</i> 1, <i>I</i> > 2σ (<i>I</i>)	0.0506	0.0441	0.0588	0.1140
<i>R</i> 1, all data	0.0744	0.0672	0.0833	0.1400
w <i>R</i> 2 (on <i>F</i> ²)	0.1563	0.1327	0.1643	0.3006
Δρ _{min} (eÅ ⁻³) close to	-0.73 W10	-0.78 Na5	-0.67 Na5	-0.82 O7
Δρ _{max} (eÅ ⁻³) close to	0.70 W8	0.90 Na5	0.80 Na5	0.81 O11

Table 2. Space group setting of Na-barrerite at 25°C and at 50°C. Non-standard setting $A2/m$ at 50°C was preferred to an easy comparison with RT data set.

space group setting	25°C		50°C	
	$C2/m$	$F2/m^*$	$C2/m$	$A2/m$
a (Å)	13.6288(2)	13.6288(2)	17.6466(3)	13.6481(2)
b (Å)	18.1600(3)	18.1600(3)	17.9357(3)	17.9357(3)
c (Å)	11.1714(2)	17.8071(4)	13.6481(2)	17.6466(3)
β (°)	127.1580(10)	90.4290(10)	90.2730(10)	90.2730(10)
V (Å ³)	2203.56(7)	4407.12(14)	4319.63(12)	4319.63(12)
*transformation matrix from $C2/m$ to $F2/m$: [100 0-10 -1 0-2]				

Table 3. Results of quantitative chemical analyses of natural barrerite as obtained from EMPA.

Mean values from 16 analytical points			
	wt. %		<i>a.p.f.u.*</i>
SiO ₂	58.40(73)	Si	54.96(24)
TiO ₂	0.16(10)	Ti	0.08(8)
Al ₂ O ₃	15.17(19)	Al	16.80(24)
Cr ₂ O ₃	0.08(10)	Cr	0.08(8)
V ₂ O ₃	0.02(4)	V	0.00
Fe ₂ O ₃	0.05(7)	Fe	0.00
MnO	0.05(7)	Mn	0.00
MgO	0.17(10)	Mg	0.24(16)
CaO	2.20(7)	Ca	2.24(8)
SrO	0.02(5)	Sr	0.00
BaO	0.22(17)	Ba	0.08(8)
Na ₂ O	4.51(15)	Na	8.24(24)
K ₂ O	2.55(10)	K	3.04(8)
NiO	0	Ni	0.00
P ₂ O ₅	0.01(3)	P	0.00
F	0.14(19)	total	85.92
Cl	0.01(1)		
Total	83.77	F ⁻	0.20(56)
E%-value	2.77		
*atoms per formula unit calculated on the basis of 144 O			

Table 4 Atomic coordinates, displacement parameters and occupancy of Na-barrerite structure under ambient conditions (T = 25°C, RH = 65%)

Framework					
Site	x	y	z	U^{eq} (Å ²)	Occ.
T1	0.36275(3)	0.30761(2)	0.12442(3)	0.01592(10)	1
T2	0.13440(3)	0.30857(2)	0.12780(3)	0.01465(10)	1
T3	-0.04995(3)	0.08891(2)	0.24713(3)	0.01565(10)	1
T4	-0.13912(3)	0.31597(2)	0.25047(3)	0.01339(9)	1
T5	½	0.24670(4)	0	0.01896(13)	1
O1	0.42803(13)	0.29989(11)	0.04649(12)	0.0359(4)	1

O2	0.06115(13)	0.30802(9)	0.05527(11)	0.0333(4)	1
O3	-0.12386(13)	0.26651(9)	0.17686(11)	0.0329(3)	1
O4	-0.10188(15)	0.11705(10)	0.16921(12)	0.0370(4)	1
O5	0.12251(12)	0.23129(9)	0.17321(10)	0.0306(3)	1
O6	0.10726(15)	0.37895(10)	0.17976(12)	0.0380(4)	1
O7	0.24616(11)	0.31801(9)	0.09743(9)	0.0287(3)	1
O8	0.06643(9)	0.11384(8)	0.24946(11)	0.0275(3)	1
O9	-0.05222(17)	0	0.25001(17)	0.0313(5)	1
O10	-1/4	0.35077(10)	1/4	0.0238(3)	1
Extraframework					
Na1	0.2497(8)	1/2	-0.0445(4)	0.050(3)	0.33(2)
Na1A	0.2938(13)	1/2	-0.0488(7)	0.059(4)	0.237(19)
Na2	-0.0852(19)	0	0.1026(15)	0.08*	0.175(11)
Na3	0.3383(12)	1/2	-0.2543(10)	0.063(5)	0.175(12)
Na4	-0.4447(15)	0.0824(9)	-0.0416(12)	0.08*	0.128(6)
Na5	-0.1787(17)	0	0.0804(10)	0.046(6)	0.126(16)
Na6	0.0766(14)	0.0785(8)	0.0496(11)	0.10*	0.196(8)
Na7	0.0225(15)	0.0745(7)	0.0266(10)	0.10*	0.353(11)
Na8	-0.1134(19)	0	0.0606(14)	0.10*	0.227(11)
Na9	0.042(3)	0	-0.074(2)	0.08*	0.116(10)
W1	0.3134(14)	1/2	-0.1729(12)	0.063(7)	0.28(3)
W2	0.2239(10)	0.3759(4)	-0.0556(5)	0.058(3)	0.46(3)
W3	0.136(2)	1/2	-0.1288(17)	0.087(11)	0.23(2)
W4	0.187(2)	1/2	-0.0432(15)	0.104(9)	0.36(3)
W5	0.346(2)	1/2	-0.1283(18)	0.120(11)	0.37(3)
W6	0.2638(11)	0.3754(4)	-0.0566(5)	0.064(3)	0.46(3)
W7	-0.2791(15)	0	0.0937(10)	0.076(6)	0.39(3)
W7A	-0.2242(16)	0	0.0864(8)	0.054(5)	0.34(3)
W8	0.0253(19)	0	0.0089(16)	0.080*	0.243(13)
W9	0.2362(17)	1/2	-0.1708(12)	0.120(8)	0.49(3)
W10	-0.3870(12)	0	0.0651(8)	0.08*	0.433(14)
*not refined					